Research Square

Preprints are preliminary reports that have not undergone peer review.
They should not be considered conclusive, used to inform clinical practice,
or referenced by the media as validated information.

Standardized Evaluation of Spatial Dose Heterogeneity in Lattice Radiotherapy Using an Ideal-Reference-Based Dual-Domain Framework

Jiajun Zheng

zhengji.ajun@163.com

Nanjing Medical University

Yuanyuan Wang

University of Science and Technology of China

Chao Li

Ruijin Hospital

Xianhu Zeng

West China Hospital of Sichuan University

Hongqiang You

Fujian Cancer Hospital

Xuezhong Ming

the Affiliated Cancer Hospital of Nanjing Medical University

Tao Zhou

the First Affiliated Hospital of USTC

Yibin Zhang

Ruijin Hospital

Ming Liu

the First Affiliated Hospital of USTC

Zhen Liu

West China Hospital of Sichuan University

Jiangping Li

West China Hospital of Sichuan University

Mingfei Pan

Nanjing Medical University

Research Article

Keywords:

Posted Date: November 17th, 2026

DOI: https://doi.org/10.21203/rs.3.rs-11469724/v1

License: This work is licensed under a Creative Commons Attribution 4.0 International License.
Read Full License

Additional Declarations: No competing interests reported.

Standardized Evaluation of Spatial Dose Heterogeneity in Lattice Radiotherapy Using an Ideal-Reference-Based Dual-Domain Framework

JIAJUN ZHENG,[1,2#*] YUANYUAN WANG,[3,4#] CHAO LI,[5] XIANHU ZENG,[6] HONGQIANG YOU,[7*] XUEZHONG MING,[2] TAO ZHOU,[4] YIBIN ZHANG,[5] MING LIU,[4] ZHEN LIU,[6] JIANGPING LI,[6] MINGFEI PAN[1]

[1]*School of Biomedical Engineering and Informatics, Nanjing Medical University, Nanjing, P.R. China.*
[2]*Department of Radiation Oncology, the Affiliated Cancer Hospital of Nanjing Medical University, Nanjing, P.R. China.*
[3]*University of Science and Technology of China, Hefei, P.R. China.*
[4]*Hefei Ion Medical Center, the First Affiliated Hospital of USTC, Division of Life Sciences and Medicine, University of Science and Technology of China, Hefei, P.R. China.*
[5]*Department of Radiation Oncology, Ruijin Hospital, Shanghai Jiaotong University School of Medicine, Shanghai, P.R. China.*
[6]*Department of Radiotherapy Physics & Technology, West China Hospital, Sichuan University, Chengdu, P.R. China.*
[7]*Department of Radiation Oncology, Clinical Oncology School of Fujian Medical University, Fujian Cancer Hospital, Fuzhou, P.R. China.*
[*] *Corresponding author: Jiajun Zheng, zhengji.ajun@163.com; Hongqiang You, youhongqiang@nuaa.edu.cn*
 # Jiajun Zheng and Yuanyuan Wang contributed equally to this work.

Abstract: **Objective:** To develop a standardized approach for quantifying spatial peak–valley dose heterogeneity in lattice radiotherapy (LRT), addressing the limitations of conventional dose-ratio metrics and the inconsistency and subjectivity of line-profile-based assessments. **Methods:** An ideal dose reference was established using the prescribed lattice geometry and peak–valley doses. Two normalized indices, N_{DVH} and N_{TLDP}, were developed to quantify volumetric and spatial deviations from the ideal reference using DVH-derived dose selectivity and geometry-defined line dose profiles, respectively. The framework was evaluated using ten phantom plans with systematically varied field numbers within three treatment modalities (IMRT, IMPT, and IMCT) and 30 multicenter plans from five clinical cases, with blinded expert rankings for comparison. A prototype was implemented using the Eclipse Scripting API (ESAPI) to assess the feasibility of integration into an existing TPS. **Results:** Across the phantom plans, N_{DVH} and N_{TLDP} ranged from 0.241 to 0.495 and from 0.396 to 0.607, respectively. Both indices generally decreased with increasing field number within each modality, whereas the conventional D_{90}/D_{10} ratio exhibited less consistent trends. Both indices were successfully calculated for all 30 multicenter plans, with positive inter-index rank correlations (ρ = 0.486–0.886). In cases with strong inter-expert agreement, index-based rankings correlated positively with expert assessments (ρ = 0.714–0.943). The ESAPI prototype enabled automated calculation, visualization, and data export. **Conclusion:** The proposed framework provides objective and complementary quantification of volumetric and spatial deviations from ideal LRT dose patterns, demonstrating preliminary applicability across different treatment techniques, lattice configurations, and institutions, with potential for TPS integration.

Keywords: Lattice radiotherapy; Standardized evaluation; Dose heterogeneity; Dual-domain framework; Ideal dose reference; Traveling salesman problem.

1. Introduction

Spatially fractionated radiation therapy (SFRT) generates a heterogeneous dose distribution characterized by alternating high-dose peaks and low-dose valleys within the target volume [1].

The unique dose pattern triggers two crucial biological phenomena: the radiation-induced bystander effect (RIBE) and the abscopal effect, which are further enhanced by vascular modulation and immune system activation in the tumor microenvironment through low-dose radiation exposure [2–4]. These synergistic mechanisms collectively contribute to enhanced response of the bulky and treatment-resistant tumors, improved local control rates, and prolonged patient survival. Lattice radiation therapy (LRT) represents a three-dimensional evolution of traditional grid SFRT, characterized by two fundamental technical aspects: (1) precise placement of multiple uniformly sized spherical dose vertices with optimized spatial distribution within the target volume, and (2) achievement of the characteristic peak-valley dose distribution through inverse planning optimization using intensity-modulated radiation therapy (IMRT), volumetric modulated arc therapy (VMAT), intensity modulated proton therapy (IMPT) and intensity modulated carbon-ion therapy (IMCT) techniques [5, 6].

Standardization remains a major challenge in LRT, encompassing lattice configuration, dose prescription, treatment planning, and clinical evaluation [7, 8]. Among these aspects, standardized reporting of dosimetric characteristics is particularly important, especially for the spatially heterogeneous peak–valley dose distributions unique to LRT. Currently, the peak-to-valley dose ratio (PVDR) is a commonly used metric for characterizing dose heterogeneity in LRT and is generally evaluated using two approaches: (1) dose–volume histogram (DVH)-based metrics and (2) representative-line dose profile (RLDP) analysis. DVH-based metrics, such as the mean dose ratio between lattice vertices and valley regions and the ratio of specific DVH dose points (D_{10}/D_{90}), provide quantitative measures of volumetric dose heterogeneity but may not characterize the three-dimensional spatial arrangement of dose peaks and valleys [9, 10]. In contrast, RLDP analysis directly visualizes spatial peak–valley dose modulation along selected sampling lines [5, 11]. However, these lines are typically defined manually, introducing observer dependence and limiting reproducibility across treatment plans and institutions. Furthermore, lattice vertices may be distributed obliquely or non-coplanarly in three-dimensional space, making conventional treatment planning systems (TPS)-based line-profile tools, which primarily operate on orthogonal image planes, insufficient for comprehensive evaluation. Therefore, an objective and standardized evaluation approach is needed to consistently characterize the volumetric and spatial dose heterogeneity of LRT.

Previous studies have highlighted the importance of consistent definitions and reporting of lattice geometry and peak–valley dose characteristics. Fan et al. compared different PVDR definitions based on dose–volume parameters and spatial sampling, demonstrating substantial variations in the resulting values and their interpretation [12]. Prado et al. proposed a vertex-pair-based valley-to-peak dose ratio (VPDR) to better characterize spatial dose modulation, representing an effort toward standardized dosimetric evaluation [13]. Despite these efforts, a consistent approach for quantitatively characterizing the overall peak–valley dose distribution remains desirable. Such an approach should provide objective and reproducible measurements based on the prescribed dose objectives and resulting dose distribution, independent of specific treatment planning techniques and observer-dependent sampling choices. Furthermore, the increasing diversity of radiotherapy technologies and TPS highlights the importance of computationally accessible methods that can be implemented across different clinical environments.

In this study, we developed an ideal-reference-based dual-domain framework for standardized evaluation of spatial dose heterogeneity of LRT. The framework quantifies volumetric deviations through a DVH-derived dose-selectivity index and spatial deviations through a geometry-defined line dose profile. Its validity was investigated through controlled phantom-based evaluations, while its applicability was further assessed using multicenter plans, with blinded expert assessments providing an independent reference. An implementation within a clinical TPS was also developed to demonstrate technical feasibility.

2. Methods

2.1. Definition of the Ideal LRT Dose Reference

LRT dose reference. For a given gross target volume (GTV), an idealized LRT reference was defined based on the prescribed lattice geometry and the corresponding peak–valley prescription scheme. The lattice structure consisted of a set of spherical vertices with predefined positions, sizes, and inter-vertex spacing. The union of all vertex volumes was referred to as the lattice region, while the remaining target volume outside the vertices was defined as the valley region. The prescribed lattice geometry and the corresponding lattice and valley regions are schematically illustrated in the left panel of Fig. 1(a). The LRT prescription aimed to deliver a uniform prescribed peak dose to the lattice region and a uniform prescribed valley dose to the valley region, thereby establishing the desired spatial peak–valley dose pattern, as schematically illustrated in the right panel of Fig. 1(a).

Ideal DVH. In the ideal LRT dose distribution, all voxels within the lattice region receive exactly the prescribed peak dose, whereas all voxels within the valley region receive exactly the prescribed valley dose. These two step-like cumulative DVHs represent the ideal volumetric dose allocation between the lattice and valley regions. The ideal relative cumulative volumes can therefore be expressed as

$$V^{\text{ideal}}_{\text{GTV}_{\text{lattice}}}(d) = \begin{cases} 1, & d \le D_{\text{P}}, \\ 0, & d > D_{\text{P}}, \end{cases} \tag{1}$$

and

$$V^{\text{ideal}}_{\text{GTV}_{\text{valley}}}(d) = \begin{cases} 1, & d \le D_{\text{V}}, \\ 0, & d > D_{\text{V}}, \end{cases} \tag{2}$$

where $V(d)$ denotes the relative cumulative volume receiving a dose equal to or greater than the dose level d, $\text{GTV}_{\text{lattice}}$ and $\text{GTV}_{\text{valley}}$ denote the lattice region and valley region, D_{P} and D_{V} denote the prescribed peak and valley doses, respectively. The resulting ideal normalized cumulative DVHs for the lattice and valley regions are illustrated in Fig. 1(b).

Ideal RLDP. Once the selected lattice vertices and their connecting sequence were determined, the dose profile sampled from the target dose distribution along the resulting representative line (RL) was defined as the RLDP. Under the ideal LRT dose distribution, each lattice segment along the representative line receives a uniform peak dose D_{P}, whereas each inter-lattice valley segment receives a uniform valley dose D_{V}. The ideal RLDP can therefore be expressed as

$$D^{\text{ideal}}_{\text{RL}}(s) = \begin{cases} D_{\text{P}}, & s \in \bigcup_{i=1}^{N} \mathcal{L}_{\text{lattice},i}, \\ D_{\text{V}}, & s \in \bigcup_{j=1}^{M} \mathcal{L}_{\text{valley},j}. \end{cases} \tag{3}$$

where $D(s)$ denotes the dose profile along the representative-line coordinate s, $\mathcal{L}_{\text{lattice},i}$ and $\mathcal{L}_{\text{valley},j}$ denote the lattice and valley segments, respectively. The resulting ideal RLDP, characterized by alternating peak- and valley-dose segments, is illustrated in Fig. 1(c).

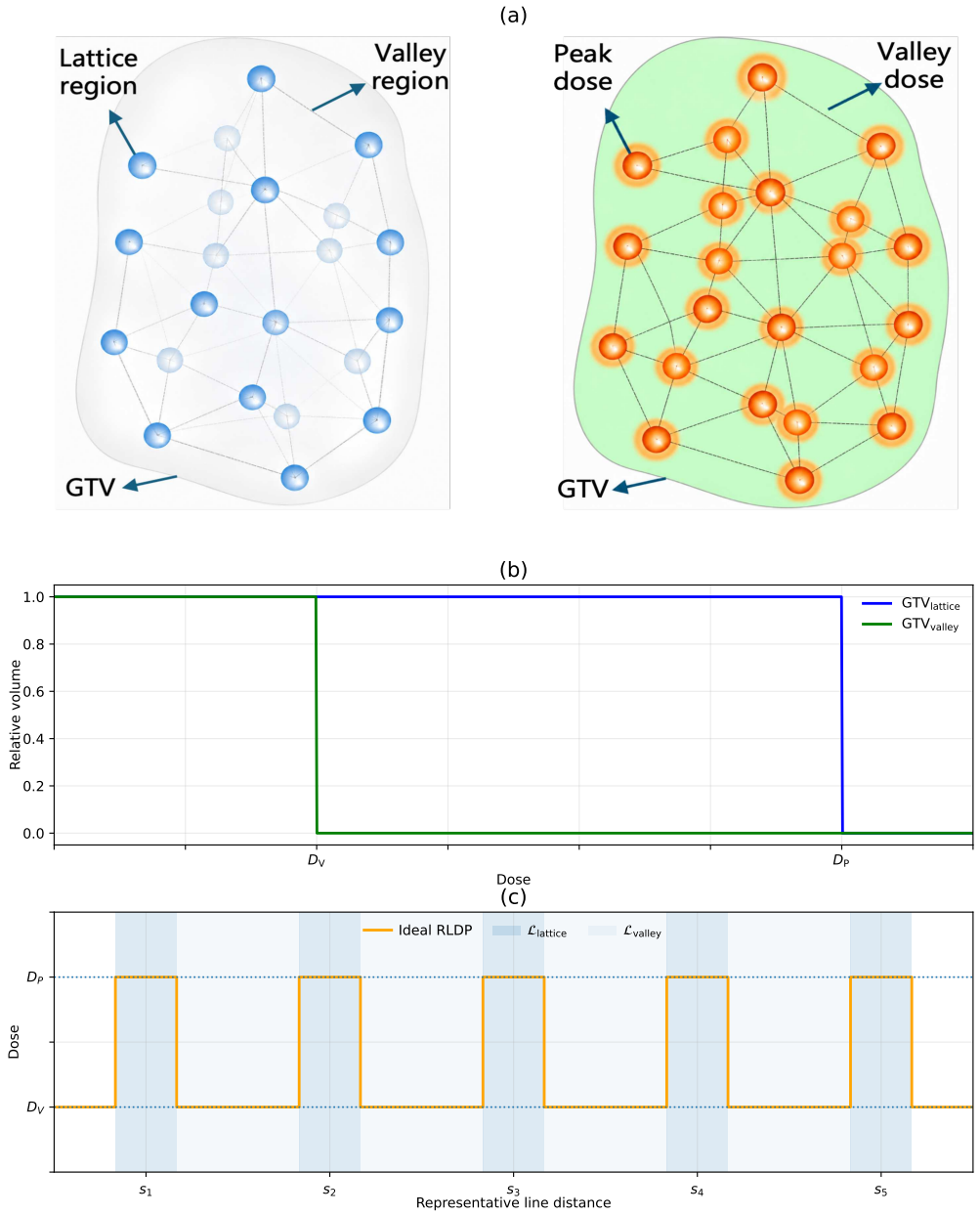


Fig. 1. Definition of ideal dose references for standardized evaluation of lattice radiotherapy. (a) Schematic illustration of the lattice geometry (left), including the GTV, lattice region, and valley region, and the corresponding ideal peak–valley dose distribution (right). (b) Ideal cumulative DVHs for the lattice and valley regions, corresponding to uniform prescribed peak and valley doses, respectively. (c) Ideal representative line dose profile (RLDP), consisting of alternating peak- and valley-dose segments along the representative line distance s.

2.2. Volumetric-domain deviation

To characterize the volumetric separation between the lattice and valley regions across the dose range, a dose-selectivity curve, $S_{\mathrm{DVH}}(d)$, was defined based on their normalized cumulative dose–volume histograms as

$$S_{\mathrm{DVH}}(d) = V_{\mathrm{GTV}_{\mathrm{lattice}}}(d) - V_{\mathrm{GTV}_{\mathrm{valley}}}(d). \tag{4}$$

The $S_{\mathrm{DVH}}(d)$ curve describes the preferential localization of dose within the lattice region relative to the valley region at each dose threshold. A positive $S_{\mathrm{DVH}}(d)$ indicates that a larger relative fraction of the lattice region than of the valley region receives at least dose d, whereas $S_{\mathrm{DVH}}(d) = 0$ indicates equal relative coverage of the two regions at that threshold. Accordingly, larger positive values indicate stronger volumetric separation between the high-dose lattice and low-dose valley regions. Because both terms are normalized to their respective regional volumes, $S_{\mathrm{DVH}}(d)$ ranges from -1 to 1. Based on the ideal LRT reference defined in Eq. 1 and 2, the corresponding ideal dose-selectivity curve is therefore

$$S_{\mathrm{DVH}}^{\mathrm{ideal}}(d) = \begin{cases} 0, & 0 \le d \le D_{\mathrm{V}}, \\ 1, & D_{\mathrm{V}} < d \le D_{\mathrm{P}}, \\ 0, & d > D_{\mathrm{P}}. \end{cases} \tag{5}$$

To quantify the overall departure of an actual dose-selectivity curve from the ideal reference, a normalized volumetric deviation index was defined as the integrated absolute difference between actual and ideal dose-selectivity curve:

$$N_{\mathrm{DVH}} = \frac{1}{D_{\mathrm{P}} - D_{\mathrm{V}}} \int_0^{d_{\max}} \left| S_{\mathrm{DVH}}^{\mathrm{actual}}(d) - S_{\mathrm{DVH}}^{\mathrm{ideal}}(d) \right| \mathrm{d}d, \tag{6}$$

where $d_{\max}$ denotes the upper dose threshold used for evaluation, and normalization by $D_{\mathrm{P}} - D_{\mathrm{V}}$ renders N_{DVH} dimensionless. An ideal dose distribution yields $N_{\mathrm{DVH}} = 0$, whereas a larger value indicates greater volumetric deviation from the prescribed ideal peak–valley dose distribution. The proposed $S_{\mathrm{DVH}}(d)$ curve and its corresponding quantitative metric N_{DVH} are schematically illustrated in Fig. 2(a) and (b), respectively.

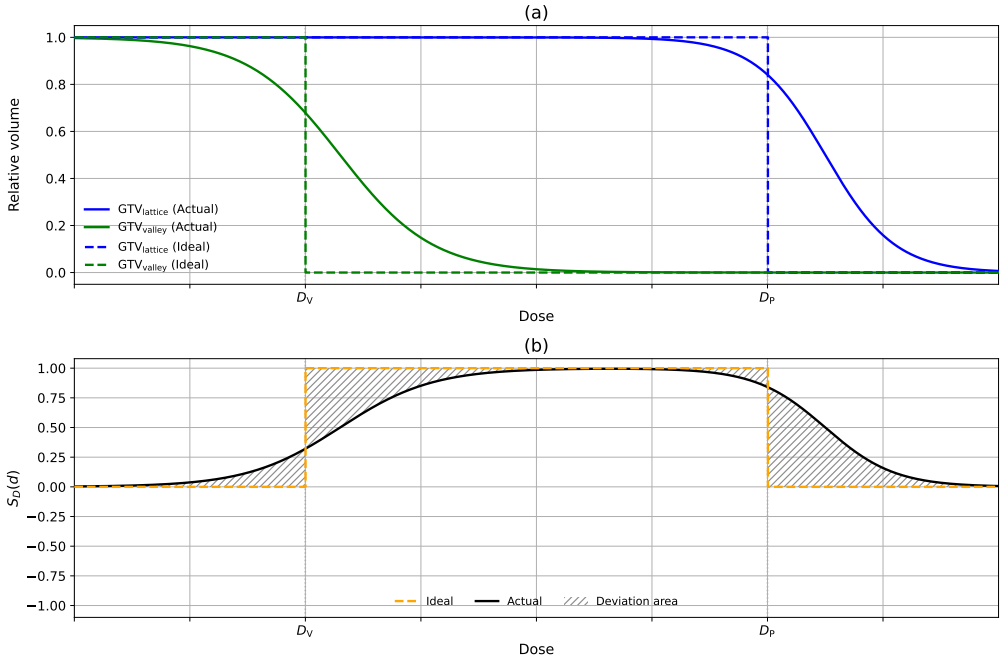


Fig. 2. Schematic illustration of the DVH-based evaluation of volumetric dose heterogeneity in lattice radiotherapy. (a) Actual and ideal cumulative DVHs for the lattice and valley regions. (b) Actual and ideal dose-selectivity curves derived from the difference between the corresponding cumulative DVHs. The hatched region represents the absolute deviation area between the actual and ideal curves, which is used to calculate the normalized DVH-based deviation metric N_{DVH}.

2.3. Spatial-domain deviation

The choice of the representative line for RLDP evaluation may be subjective and may not include all lattice vertices. To obtain a reproducible and geometry-defined dose profile, we constructed a specific representative line as a polyline sequentially connecting the centers of all lattice vertices. The ordering of vertices along the polyline was determined by solving an open traveling salesman problem (open-TSP) [14, 15], where the optimal sequence $\boldsymbol{\pi}^*$ was obtained by minimizing the total Euclidean polyline length:

$$\boldsymbol{\pi}^* = \arg\min_{\boldsymbol{\pi}} \sum_{i=1}^{N-1} \left\| \mathbf{c}_{\pi_{i+1}} - \mathbf{c}_{\pi_i} \right\|_2 . \tag{7}$$

where $\mathbf{c}_i$ denotes the three-dimensional coordinate vector of the i-th lattice vertex center, π_i denotes the ordering of the i-th vertice along the polyline, $\|\mathbf{c}_{\pi_{i+1}} - \mathbf{c}_{\pi_i}\|_2$ represents the Euclidean distance between two consecutive vertices along the polyline, and N is the total number of lattice vertices.

The open-TSP was approximately solved using a multi-start nearest-neighbor heuristic followed by 2-opt refinement. The computational procedure consisted of the following steps:

1. **Vertex center extraction:** The three-dimensional coordinates of all lattice vertex centers were extracted.

2. **Distance matrix construction:** Pairwise Euclidean distances between vertex centers were calculated to construct the distance matrix.

3. **Nearest-neighbor initialization:** Starting from different vertices, an initial open path was constructed by iteratively connecting the nearest unvisited vertex.

4. **2-opt refinement:** Each candidate path was refined by iteratively reversing subsequences of the vertex ordering to reduce the total Euclidean path length.

5. **Optimal candidate selection:** The candidate path with the shortest total length was selected as the final optimized solution.

6. **Vertex ordering output:** The optimized vertex sequence was recorded for subsequent dose-profile sampling and analysis.

The optimized polyline generated using the open-TSP method was defined as the TSP-line (TL) for RLDP evaluation, which connects all lattice vertex centers while minimizing the total path length, as illustrated in Fig. 3(a). The dose profile sampled from the target dose distribution along TSP-line was termed the TSP-line dose profile (**TLDP**).

The deviation between the TLDP of actual dose distribution and ideal TLDP defined in Eq. 3 was quantified by integrating the absolute dose differences along the entire TSP-line, and normalized by the ideal peak–valley dose integral:

$$N_{\mathrm{TLDP}} = \frac{1}{D_{\mathrm{P}} L_{\mathcal{L}_{\mathrm{lattice}}} + D_{\mathrm{V}} L_{\mathcal{L}_{\mathrm{valley}}}} \int_0^{L_{\mathrm{TL}}} \left| D_{\mathrm{TL}}^{\mathrm{actual}}(s) - D_{\mathrm{TL}}^{\mathrm{ideal}}(s) \right| \, \mathrm{d}s, \tag{8}$$

where L_{TL}, L_{lattice} and L_{valley} represent the total length of the TL, lattice and valley segments. The numerator represents the absolute deviation area between the actual and ideal TLDPs, as illustrated by the hatched region in Fig. 3(b). The denominator corresponds to the ideal peak–valley dose integral along the TL and normalizes the metric, making N_{TLDP} dimensionless. An ideal spatial dose distribution yields $N_{\mathrm{TLDP}} = 0$, whereas larger values indicate greater deviation from the prescribed peak–valley pattern.

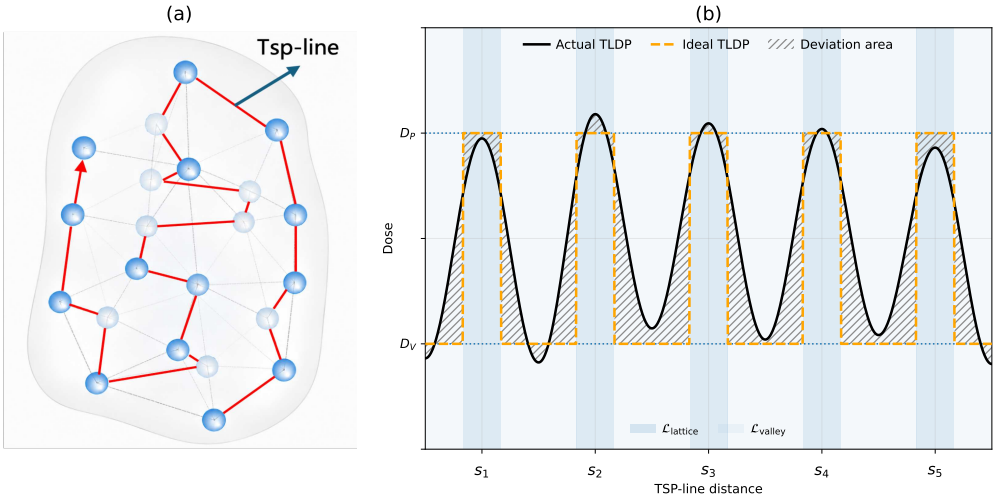


Fig. 3. Schematic illustration of the TSP-line dose profile (TLDP) evaluation framework. (a) Construction of the TSP-line (TL) using the open traveling salesman problem (open-TSP) method, which connects all lattice vertex centers while minimizing the total path length. (b) Actual and ideal TLDPs obtained by sampling the corresponding three-dimensional dose distributions along the TL. The hatched region represents the absolute deviation between the actual and ideal TLDPs, which is used to calculate the normalized dose-profile deviation metric N_{TLDP}.

2.4. Phantom-based validation

A homogeneous cylindrical solid-water phantom, 27 cm in diameter and 27 cm in height, was simulated as a CT image dataset with a 2-mm slice thickness to represent a simplified patient geometry. A synthetic GTV was constructed as the union of four partially overlapping spheres with radii of 7.0, 4.4, 3.6, and 2.8 cm, corresponding to a total volume of 1816 cc and an equivalent diameter of 15.1 cm. The sphere centers were initially positioned at $(0, 0, 0)$, $(7, 0, 0)$, $(0, 7, 0)$, and $(0, 0, 7)$ cm, respectively, followed by sequential 45° rotations of the composite GTV about the x-, y-, and z-axes. The resulting target geometry was asymmetric and orientation-dependent, providing a suitable configuration for validation of the dual-domain framework. Lattice vertices with a diameter of 1 cm were generated and distributed within the synthetic GTV using a center-to-center spacing of 3 cm, resulting in a total of 50 vertices ($N_{\text{P}} = 50$). The geometric configuration of the phantom, synthetic GTV, and lattice vertices is illustrated in Fig. 4. The prescribed peak dose was 67.5 Gy(RBE) in 5 fractions ($D_{\text{P}} = 67.5$), whereas the dose outside the lattice vertices was minimized toward a prescribed valley dose of 20 Gy(RBE) in 5 fractions ($D_{\text{V}} = 20$) [16].

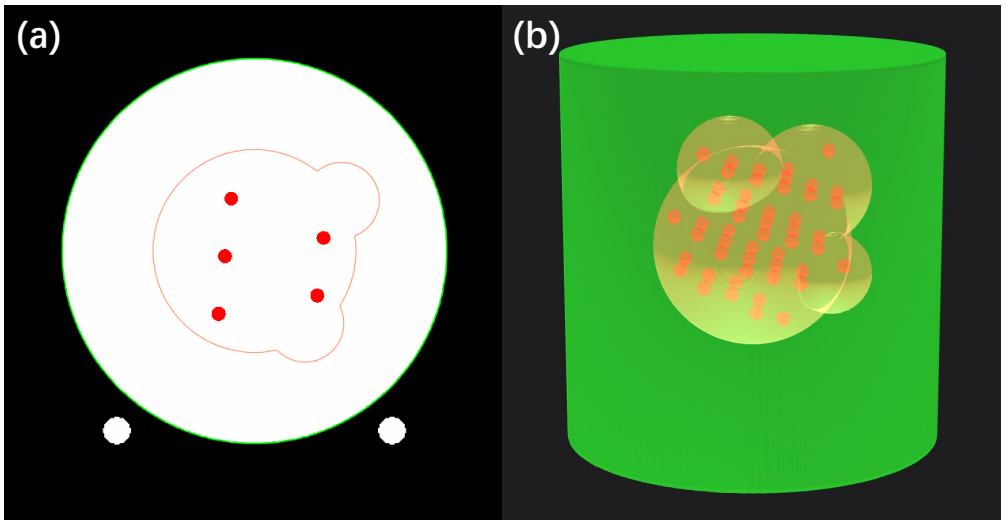


Fig. 4. Geometric configuration of the phantom (green), synthetic GTV (orange), and lattice vertices (red) used for validation of the dual-domain framework in the axial view (a) and three-dimensional view (b).

Three treatment-technique families, IMRT, IMPT, and IMCT, were investigated to generate controlled variations in spatial dose modulation through systematic variation of the number of irradiation fields. For IMRT, plans with 7, 9, 12, and 15 fields were developed using Eclipse TPS (v15.6, Varian Medical Systems, USA), based on a beam model of a TrueBeam linear accelerator (Varian Medical Systems, USA). For IMPT, plans with 1, 2, 3, and 4 fields were generated using CuraProton TPS (v1.0, Raynaissance, China) [17], based on a beam model of the Varian ProBeam system equipped with a 360° rotating gantry (Varian Medical Systems, USA) [18]. For IMCT, plans with single lateral (1) field and opposed lateral (2) fields were generated using Phoenix Plan TPS (CAS Ion Ltd., China), based on a beam model of the Heavy Ion Medical Machine (HIMM) system equipped with a horizontal fixed beamline [19]. Photon, proton, and carbon-ion doses were all expressed in Gy(RBE). A constant RBE of 1.0 was adopted for photon plans, and an RBE of 1.1 was assumed for proton plans. For carbon-ion plans, RBE-weighted dose distributions were calculated using the linear–quadratic (LQ)-based RBE model implemented in the TPS, which incorporates LET-dependent biological parameters, voxel-wise physical dose, and dose-averaged LET ($\mathrm{LET_d}$) [20]. Within each technique family, identical optimization objectives and dose calculation settings were maintained, while only the number of irradiation fields was varied. All plans were normalized such that 100% of the prescribed peak dose covered 95% of the lattice region. Neither IMPT nor IMCT plans employed robust optimization. A total of ten plans were therefore generated for dual-domain evaluation and were not delivered on a physical treatment system.

For each plan, the lattice and valley cumulative DVHs were first calculated, and the corresponding dose-selectivity curve, $S_{\mathrm{DVH}}(d)$, was derived according to Eq. (4). The normalized volumetric deviation, N_{DVH}, was then calculated from the integrated absolute difference between the actual and ideal $S_{\mathrm{DVH}}(d)$ curves according to Eq. (6). For the given GTV and lattice configuration, a single TSP-line was generated by optimizing the ordering of all lattice vertex centers using the open-TSP method, according to Eq. (7). Each three-dimensional dose distribution was sampled along the TSP-line using trilinear interpolation to obtain the TLDP, from which the normalized spatial deviation, N_{TLDP}, was calculated according to Eq. (8). The behavior of N_{DVH} and N_{TLDP} was evaluated across the controlled IMRT, IMPT and IMCT plan series to assess the response of

the proposed volumetric- and spatial-domain metrics to systematic changes in irradiation-field number. As a conventional DVH-based comparator, the dose ratio D_{90}/D_{10} of the GTV was additionally calculated. This ratio was used only as a reference metric and was not considered part of the proposed dual-domain framework. Previously reported RLDP-based metrics were not included as conventional comparators because the selection of representative lines and calculation procedures were not consistently standardized across studies.

2.5. Multicenter clinical validation

2.5.1. Clinical cases

Five clinical cases with bulky tumors in different anatomical sites were retrospectively selected and distributed to four participating institutions for independent LRT planning. Planning CT images were acquired using a Siemens CT scanner (Siemens Healthcare, Germany) with a uniform slice thickness of 2 mm. The GTVs were delineated by experienced radiation oncologists. The anatomical sites, GTV characteristics, lattice geometry, and predefined prescription scheme for multicenter planning are summarized in Table 1, with the prescription scheme adapted from Ferini et al. [21].

Table 1. Anatomical sites, GTV characteristics, lattice geometry, and predefined prescription scheme of five cases for multicenter LRT planning.

Case	Site	GTV characteristics		Lattice geometry			Prescription
		diameter	volume	distance	diameter	N_P	D_P / D_V
#01	H&N	9.5 cm	434 cc	3 cm	1 cm	6	15 / 0 Gy
#02	lung	11.6 cm	813 cc	3 cm	1 cm	19	15 / 0 Gy
#03	liver	9.4 cm	429 cc	3 cm	1 cm	7	15 / 0 Gy
#04	H&N	15.3 cm	1865 cc	4 cm	1 cm	14	15 / 0 Gy
#05	extremity	13.5 cm	1292 cc	4 cm	1 cm	16	15 / 0 Gy

2.5.2. Multicenter planning protocol

All centers received the same CT datasets, target delineations, and predefined lattice structures, and were required to satisfy the predefined prescription requirements while considering clinical feasibility. According to the standardized planning protocol, each participating institution was encouraged to submit its best achievable LRT plan for each treatment modality currently available or expected to become available at that institution, using its established or prospective clinical planning workflow and treatment platform. Photon LRT plans could be generated using institution-specific IMRT, VMAT, or tomotherapy techniques, whereas proton LRT plans could be generated using clinically available IMPT or proton arc-based approaches. All planning parameters, including the beam arrangement, optimization objectives, organ at risk (OAR) constraints, proton robust optimization settings, and delivery time, were determined according to each institution's clinical planning protocol.

2.5.3. Blinded expert assessment

A blinded expert assessment was performed to provide an independent clinical evaluation of the spatial peak–valley dose patterns. For each clinical case, the dose distributions of all submitted plans were displayed simultaneously in a multi-panel video, allowing direct visual comparison

of the spatial dose patterns across different plans. All plans were anonymized and randomly arranged before review, and the participating experts were blinded to the treatment institution, planning technique, and quantitative dosimetric indices. Based solely on visual inspection of the dose distributions, the experts independently ranked the submitted plans according to the perceived quality of spatial peak–valley dose modulation.

2.5.4. Evaluation endpoint

For each submitted plan, the volumetric-domain deviation index N_{DVH} and spatial-domain deviation index N_{TLDP} were calculated using the proposed dual-domain framework. The submitted plans were ranked separately according to each quantitative metric, and the resulting rankings were compared with those obtained from the blinded expert assessment to evaluate the agreement between quantitative dosimetric evaluation and expert judgment.

2.6. Technical Integration

To assess the feasibility of integrating the proposed dual-domain evaluation framework into a clinical TPS, a prototype was developed using the Eclipse Scripting API (ESAPI, Varian Medical Systems, USA). The implementation automatically retrieved the treatment plan, dose distribution, and predefined lattice and valley structures. The corresponding cumulative DVHs were extracted to generate $S_{\mathrm{DVH}}(d)$ and calculate N_{DVH}. For spatial-domain evaluation, individual lattice vertex centers were identified from the three-dimensional structure geometry and connected using an open-TSP-based optimization procedure. Dose values were sampled along the resulting TSP-line at 0.5-mm intervals to generate the TLDP and calculate N_{TLDP}. A graphical interface was developed for visualization of the evaluation results and export of the corresponding quantitative data.

3. Results

3.1. Dosimetric Performance

Fig. 5 illustrates the representative application of the proposed dual-domain framework to the IMPT-1F phantom plan. The three-dimensional dose distribution showed the characteristic heterogeneous lattice pattern, with high-dose regions localized around the predefined lattice vertices. The cumulative DVHs of the lattice and valley regions demonstrated clear volumetric dose separation, while the open-TSP procedure generated a continuous three-dimensional path (TSP-line) sequentially connecting all lattice vertex centers.

The corresponding dose-selectivity curve deviated from the ideal step-like reference over both the transition and high-dose regions, resulting in a normalized volumetric deviation of $N_{\mathrm{DVH}} = 0.4405$. In the spatial domain, the TLDP preserved the sequential peak–valley pattern along the predefined path but showed departures from the ideal peak and valley dose levels, yielding a normalized spatial deviation of $N_{\mathrm{TLDP}} = 0.4962$. These results demonstrate that the proposed framework provides complementary volumetric- and spatial-domain quantification of the deviation from the prescribed ideal LRT dose pattern within the same treatment plan.

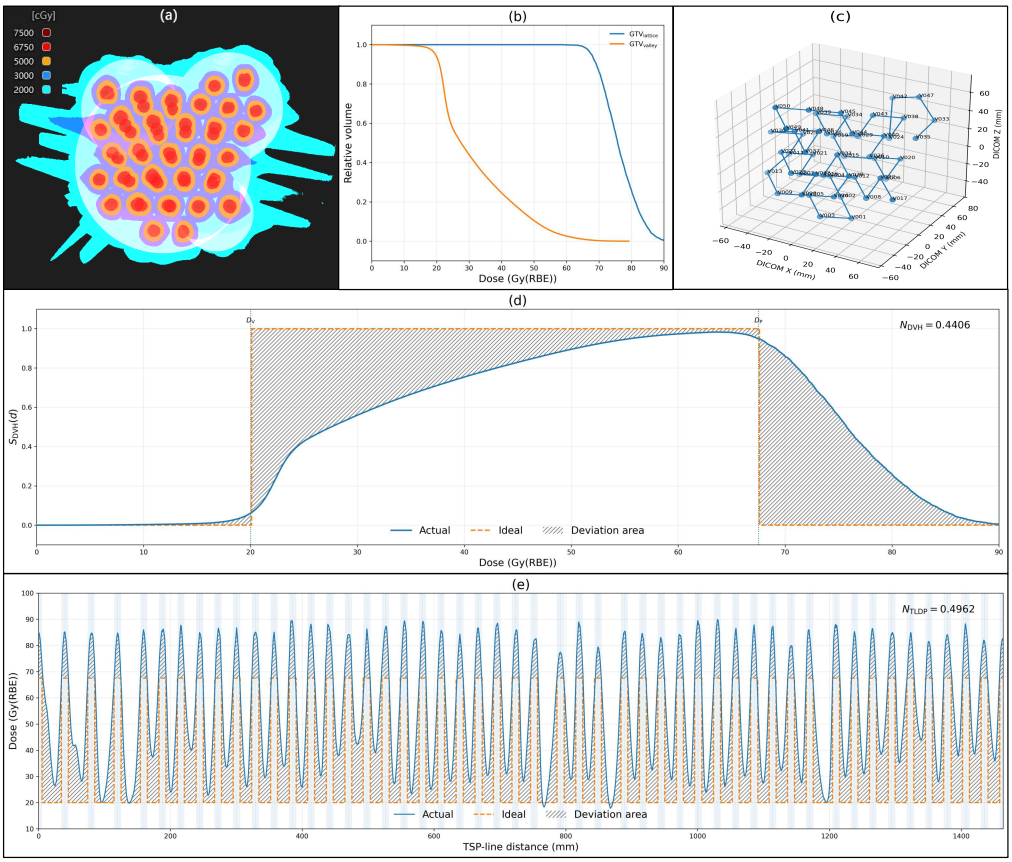


Fig. 5. Representative application of the proposed ideal-reference-based dual-domain framework to the IMPT-1F phantom plan. (a) Three-dimensional dose distribution showing the heterogeneous lattice dose pattern. (b) Normalized cumulative dose–volume histograms (DVHs) of the lattice and valley regions. (c) Three-dimensional TSP-line generated using the open-TSP method to sequentially connect all lattice vertex centers for TSP-line dose profile (TLDP) evaluation. (d) Actual and ideal dose-selectivity curves with the hatched area representing the volumetric deviation used to calculate N_{DVH}. (e) Actual and ideal TLDPs, with the hatched area representing the spatial deviation used to calculate N_{TLDP}.

As shown in Fig. 6(a), the volumetric-domain deviation N_{DVH} decreased from 0.495 for IMRT-7F to 0.427 for IMRT-15F, with modest intermediate variations. A more pronounced and systematic reduction was observed across the IMPT series, with N_{DVH} decreasing from 0.441 for IMPT-1F to 0.241 for IMPT-4F. The IMCT plans exhibited intermediate values, decreasing from 0.361 for IMCT-1F to 0.337 for IMCT-2F. A similar but not identical pattern was observed for the spatial-domain deviation N_{TLDP} [Fig. 6(b)]. N_{TLDP} decreased progressively from 0.496 to 0.396 as the number of IMPT fields increased from one to four, whereas the IMRT series showed comparatively smaller variations, with values ranging from 0.607 to 0.576. In contrast, N_{TLDP} increased slightly from 0.456 to 0.460 between IMCT-1F and IMCT-2F, despite the reduction in N_{DVH}. Overall, the two proposed indices exhibited broadly consistent trends across different treatment modalities and beam configurations, generally decreasing with increasing numbers of irradiation fields within each modality, albeit with minor differences in their detailed responses.

The conventional DVH-based ratio D_{90}/D_{10} exhibited different trends from the proposed deviation indices [Fig. 6(c)]. For example, IMPT-1F showed the lowest D_{90}/D_{10} among the IMPT plans, whereas its N_{DVH} and N_{TLDP} were both higher than those of the multi-field IMPT plans. These findings indicate that the conventional single-value DVH ratio and the proposed ideal-reference-based deviation indices characterize different aspects of heterogeneous LRT dose distributions.

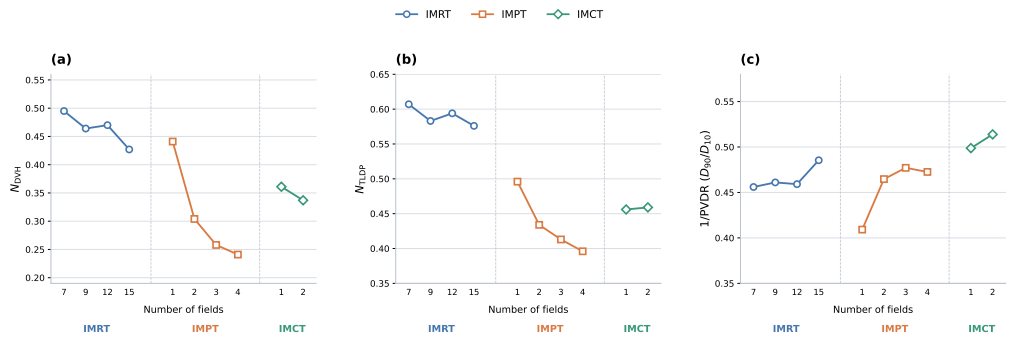


Fig. 6. Comparison of dosimetric indices among intensity-modulated radiotherapy (IMRT), intensity-modulated proton therapy (IMPT), and intensity-modulated carbon-ion therapy (IMCT) plans with different numbers of irradiation fields. (a) Volumetric-domain deviation index (N_{DVH}); (b) spatial-domain deviation index (N_{TLDP}); and (c) conventional dose ratio (D_{90}/D_{10}). Lower values of N_{DVH} and N_{TLDP} indicate smaller deviations from the corresponding ideal LRT references.

3.2. Multicenter Plan Evaluation

A total of 30 LRT plans were collected for five clinical cases from four participating institutions, with six plans submitted for each case. Institution 1 submitted a conventional IMPT plan, whereas Institution 4 employed the emerging proton arc therapy technique, neither of which incorporated robust optimization. Institutions 2 and 3 each submitted both VMAT and IMPT plans, with different robust optimization settings applied to their proton plans. Beam configurations, including field numbers and orientations, as well as organ-at-risk (OAR) constraints, varied across institutions according to their respective planning strategies. The TPSs included Eclipse, RayStation, and CuraProton, while the treatment delivery systems comprised Varian TrueBeam and ProBeam, as well as synchrotron-based proton system SAPT-PS-01. The participating planners had 3–10 years of clinical experience. Collectively, these variations yielded a heterogeneous set of LRT plans encompassing different treatment modalities, planning systems, and optimization strategies. Both

proposed indices, N_{DVH} and N_{TLDP}, were successfully calculated for all 30 plans, and the plans were independently ranked according to their respective index values. Two senior experts from different institutions, comprising an experienced radiation oncologist and a medical physicist, independently reviewed the plans and submitted their rankings. The individual dosimetric index values, corresponding plan rankings, and expert assessments for all 30 plans are provided in Supplementary Table S1.

Table 2 summarizes the pairwise Spearman rank correlations among the two proposed indices and the blinded expert assessments across the five clinical cases. The rankings derived from N_{DVH} and N_{TLDP} showed positive correlations in all cases, with coefficients ranging from 0.486 to 0.886. Strong inter-expert agreement was observed in #02, #03, and #04 (ρ = 0.943–1.000), whereas lower agreement was found in #01 and #05 (ρ = 0.486 and 0.429, respectively). In the three cases with strong inter-expert agreement, both proposed indices generally showed positive correlations with the expert rankings, with coefficients ranging from 0.714 to 0.943. In contrast, the two cases with lower inter-expert agreement exhibited greater variability in index–expert correlations. For #01, both indices showed stronger agreement with Expert 2 than with Expert 1. Similarly, in #05, N_{TLDP} showed substantially higher agreement with Expert 2 than N_{DVH} (ρ = 0.886 vs. 0.200).

Table 2. Pairwise Spearman rank correlations among the proposed dosimetric indices and blinded expert assessments across five clinical cases.

Case	Inter-index	Inter-expert	Index–expert correlations			
	N_{DVH}–N_{TLDP}	E1–E2	N_{DVH}–E1	N_{TLDP}–E1	N_{DVH}–E2	N_{TLDP}–E2
#01	0.886	0.486	0.543	0.314	0.943	0.771
#02	0.829	1.000	0.943	0.714	0.943	0.714
#03	0.829	0.943	0.886	0.714	0.943	0.771
#04	0.886	0.943	0.829	0.886	0.943	0.943
#05	0.486	0.429	0.371	0.543	0.200	0.886

N_{DVH} and N_{TLDP} denote rankings based on their values, respectively. E1 and E2 denote Expert 1 and Expert 2. All values represent Spearman's rank correlation coefficient (ρ), calculated across six plans within each case.

3.3. TPS Integration

The proposed dual-domain evaluation framework was successfully implemented as an ESAPI-based prototype within the Eclipse TPS. As illustrated in Fig. 7, the interface integrates patient and plan (a nine-fields IMRT plan of #03) information, actual and ideal cumulative DVHs of the lattice and valley regions, and the corresponding dose-selectivity curves with the calculated N_{DVH}. The three-dimensional TSP-line is displayed alongside the actual and ideal TLDPs and the corresponding N_{TLDP}. The evaluation results and sampled dose-profile data can be exported for subsequent analysis.



Fig. 7. TPS-integrated implementation of the proposed dual-domain dosimetric evaluation framework using the Eclipse Scripting API (ESAPI). The interface displays lattice and valley DVHs, the dose-selectivity curve, the three-dimensional TSP-line, and the TLDP, together with the corresponding deviation indices.

4. Discussion

This study developed an ideal-reference-based dual-domain framework for standardized dosimetric evaluation of lattice radiotherapy. By defining the prescribed peak–valley dose pattern as a common reference, the proposed framework quantifies deviations in both volumetric and spatial domains through two complementary indices, N_{DVH} and N_{TLDP}. Unlike conventional DVH-based parameters or manually selected line profiles, the framework incorporates an explicit reference distribution and a geometry-defined three-dimensional sampling path, enabling reproducible assessment of dose heterogeneity. Its applicability was demonstrated through phantom-based comparisons across photon, proton, and carbon-ion techniques, multicenter clinical plan evaluations, and implementation within a clinical TPS.

The physical rationale of the proposed indices was examined through two complementary evaluation approaches. In the phantom study, the number of irradiation fields was systematically increased within each treatment-technique family while other planning settings were maintained. Based on established treatment planning principles, increasing the number of fields was expected to provide greater flexibility in dose modulation and improve peak–valley dose separation. As shown in Fig. 6(a) and (b), both N_{DVH} and N_{TLDP} generally decreased with increasing field number, consistent with this physically motivated expectation. In contrast, the conventional (D_{90}/D_{10}) ratio exhibited less consistent trends [Fig. 6(c)], reflecting the limitations of characterizing complex dose heterogeneity using only two DVH dose quantiles. The multicenter evaluation provided complementary evidence through blinded expert assessments. In cases with strong inter-expert agreement (#02–#04), rankings derived from both indices generally aligned with expert judgments, supporting their relevance to peak–valley dose evaluation. Conversely, lower inter-expert agreement in cases #01 and #05 was accompanied by greater variability in

index–expert correlations, potentially reflecting differences in experts' tolerance for deviations from the prescribed high-dose pattern at lattice vertices. Together, these findings provide preliminary support for the physical relevance of the proposed indices, although neither increased field number nor expert judgment constitutes an absolute ground truth for plan quality.

The generalizability of the proposed framework is supported by several features of the evaluation design. First, the phantom and multicenter clinical cases encompassed different anatomical sites, target volumes, lattice geometries, vertex numbers, and peak–valley prescription schemes, including 67.5/20 Gy(RBE) in five fractions for the phantom plans and 15/0 Gy(RBE) in single fraction for the clinical plans. Despite these differences, both indices were calculated using identical mathematical definitions, with normalization accounting for the prescribed dose levels and corresponding spatial characteristics. Second, the evaluated plans covered photon, proton, and carbon-ion techniques, together with variations in beam configurations, optimization strategies, planning systems, institutional protocols, and planner experience. Because the framework relies on the prescribed lattice configuration, peak–valley dose levels, and final three-dimensional dose distribution, its calculation does not require modality-specific beam parameters or delivery characteristics. Third, the predefined dose reference and geometry-driven TSP-line reduce dependence on manually selected sampling locations and directions, providing an objective and consistent basis for evaluation across observers. Furthermore, because the TSP-line is defined independently of the sampled physical quantity, the same geometric sampling strategy could potentially be extended to $\mathrm{LET_d}$ distributions, which have attracted increasing attention in proton and carbon-ion radiotherapy [22, 23]. Such an extension could complement LET–volume histogram (LVH)-based evaluation by providing additional information on the spatial localization of $\mathrm{LET_d}$ relative to lattice vertices, although dedicated reference definitions and validation would be required. Collectively, these characteristics support the applicability of the framework across different lattice configurations, prescription schemes, treatment techniques, and institutions, while systematic comparisons remain necessary to establish the equivalence of index interpretation across substantially different conditions.

The proposed framework is applicable to lattice configurations with either uniform or nonuniform vertex sizes, provided that the dimensions of individual vertices are predefined and incorporated into the geometric representation during implementation. Importantly, both indices are defined with respect to a given lattice configuration and prescribed peak–valley dose scheme. Accordingly, the framework is intended for evaluating and comparing treatment plans under the same target geometry, lattice configuration, and prescription, rather than for direct quantitative comparisons across different clinical cases or inconsistent lattice and prescription settings.

Beyond its general applicability, the proposed framework offers practical advantages in computational implementation. Its underlying procedures are relatively straightforward and transparent, comprising conventional DVH analysis, three-dimensional geometric calculations, open-TSP-based path optimization, and numerical integration, without requiring complex predictive models or model training. This simplicity facilitates software implementation and adaptation to different TPS environments. As demonstrated by the ESAPI-based prototype, the framework can be integrated into an existing treatment planning workflow for automated calculation, visualization, and export of the dual-domain evaluation results. Similar implementations could be developed through the scripting or software interfaces of other mainstream TPSs, such as RayStation and Monaco [24, 25], without modifying the underlying mathematical framework. These features provide a practical basis for broader deployment, although numerical consistency between independent TPS implementations remains to be verified.

Several limitations of this study should be acknowledged. First, the ideal reference adopts a simplified peak–valley dose pattern with uniform dose levels and sharply defined boundaries. In clinical practice, however, dose transition regions between lattice vertices and surrounding valleys are unavoidable, while reductions in vertex doses may be clinically justified by organ-

at-risk constraints. Future studies should therefore explore more clinically informed reference distributions that incorporate dose gradients and acceptable deviations from prescribed peak doses. Second, the TSP-line may introduce spatial sampling bias because a single trajectory cannot fully represent the three-dimensional dose distribution. Nevertheless, by connecting lattice vertex centers along a geometrically optimized shortest path, the TSP-line naturally traverses the intervening valley regions between successive vertices, potentially capturing unfavorable peak–valley dose separation. Whether this sampling strategy reliably captures the most unfavorable peak–valley dose characteristics requires further systematic investigation. Third, the phantom evaluation was limited to a single synthetic target configuration, while the multicenter assessment included only five clinical cases and two experts. Furthermore, although the ESAPI-based prototype demonstrated implementation feasibility, numerical consistency across different TPS platforms remains to be established. Future studies involving larger multicenter datasets, diverse lattice configurations, and independent cross-platform implementations are warranted to further assess the reproducibility, robustness, and generalizability of the proposed framework.

5. Conclusion

This study developed an ideal-reference-based dual-domain framework for standardized dosimetric evaluation of lattice radiotherapy. The proposed indices, N_{DVH} and N_{TLDP}, provide complementary quantification of volumetric and spatial deviations from the prescribed peak–valley dose pattern. Phantom-based and multicenter evaluations provided preliminary support for their physical relevance and applicability across different lattice configurations, prescription schemes, treatment modalities, and institutions. Furthermore, the ESAPI-based implementation demonstrated the feasibility of integrating the framework into clinical treatment planning systems. The proposed framework offers an objective, reproducible, and potentially transferable approach to standardized LRT dosimetric evaluation.

6. Declarations

Abbreviations. SFRT: spatially fractionated radiation therapy; RIBE: radiation-induced bystander effect; LRT: lattice radiation therapy; IMRT: intensity-modulated radiation therapy; VMAT: volumetric modulated arc therapy; IMPT: intensity modulated proton therapy; IMCT: intensity modulated carbon-ion therapy; PVDR: peak-to-valley dose ratio; DVH: dose-volume histogram; RLDP: representative-line dose profile; TPS: treatment planning systems; TSP: traveling salesman problem; TL: TSP-line; TLDP: TSP-line dose profile; HIMM: Heavy Ion Medical Machine; LET: linear energy transfer; OAR: organ at risk; ESAPI: Eclipse Scripting Application Programming Interface.

Ethics approval and consent to participate. This study was approved by the Ethics Committee of the Affiliated Cancer Hospital of Nanjing Medical University and was conducted in accordance with the Declaration of Helsinki, and the requirement for informed consent was waived due to the retrospective nature of the study and the use of anonymized data.

Consent for publication. Not Applicable.

Availability of data and materials. The datasets generated and/or analyzed during the current study are not publicly available due to ethical restrictions and patient privacy considerations, but are available from the corresponding author on reasonable request.

Competing Interests. The authors declare that they have no known competing financial interests or personal relationships that could have appeared to influence the work reported in this paper.

Funding. This work was funded by the Spark Basic Research Program of the Affiliated Cancer Hospital of Nanjing Medical University (No. ZJ202309) and Anhui Province Special Project on Clinical Medical Research (No. 202527c10020134).

Author's Contributions.

Jiajun Zheng: Conceptualization, Methodology, Software, Formal analysis, Validation, Visualization, Investigation, Data curation, Writing – original draft, Writing – review and editing, Project administration. Yuanyuan Wang: Methodology, Investigation, Validation, Data curation, Writing – review and editing. Chao Li: Software, Formal analysis, Data curation. Xianhu Zeng: Investigation, Resources, Data curation. Hongqiang You: Supervision, Methodology, Writing – review and editing. Xuezhong Ming: Investigation, Resources, Validation. Tao Zhou: Investigation, Resources, Data curation. Yibin Zhang: Investigation, Visualization, Data curation. Ming Liu: Investigation, Resources, Validation. Zhen Liu: Investigation, Resources, Validation. Jiangping Li: Investigation, Resources, Data curation. Mingfei Pan: Investigation, Resources, Data curation.

Acknowledgments.

The authors gratefully acknowledge Yifei Xu of Raynaissance (China) and Kai Wang of CAS Ion Ltd. (China) for their technical support and assistance with the CuraProton and Phoenix Plan treatment planning systems, respectively. The authors also thank all participating institutions and colleagues for their valuable contributions and support throughout this study.

References

1. M. Mohiuddin, M. Fujita, W. F. Regine, *et al.*, "High-dose spatially-fractionated radiation (grid): a new paradigm in the management of advanced cancers," Int. J. Radiat. Oncol. Biol. Phys. **45**, 721–727 (1999).
2. C. Billena and A. J. Khan, "A current review of spatial fractionation: Back to the future?" Int. J. Radiat. Oncol. Biol. Phys. **104**, 177–187 (2019).
3. W. Yan, M. K. Khan, X. Wu, *et al.*, "Spatially fractionated radiation therapy: History, present and the future," Clin. translational radiation oncology **20**, 30–38 (2020).
4. H. Li, N. A. Mayr, R. J. Griffin, *et al.*, "Overview and recommendations for prospective multi-institutional spatially fractionated radiation therapy clinical trials," Int. J. Radiat. Oncol. Biol. Phys. **119**, 737–749 (2024).
5. X. Wu, M. M. Ahmed, J. Wright, *et al.*, "On modern technical approaches of three-dimensional high-dose lattice radiotherapy (lrt)," Cureus **2** (2010).
6. F. Iori, A. Cappelli, E. D'Angelo, *et al.*, "Lattice radiation therapy in clinical practice: A systematic review," Clin. Transl. Radiat. Oncol. **39**, 100569 (2023).
7. C. S. Mayo, J. M. Moran, W. Bosch, *et al.*, "American association of physicists in medicine task group 263: standardizing nomenclatures in radiation oncology," Int. J. Radiat. Oncol. Biol. Phys. **100**, 1057–1066 (2018).
8. N. A. Mayr, M. Mohiuddin, J. W. Snider, *et al.*, "Practice patterns of spatially fractionated radiation therapy: a clinical practice survey," Adv. Radiat. Oncol. **9**, 101308 (2024).
9. S. Mossahebi, J. K. Molitoris, Y. Poirier, *et al.*, "Clinical implementation and dosimetric evaluation of a robust proton lattice planning strategy using primary and robust complementary beams," Int. J. Radiat. Oncol. Biol. Phys. **120**, 1149–1158 (2024).
10. Y. Qian, Y. Jia, Q. Fan, *et al.*, "A novel lattice technique via adaptive spot assignment and let optimization based proton arc therapy," Int. J. Radiat. Oncol. Biol. Phys. (2026).
11. M. P. Grams, H. S. W. C. Tseung, S. Ito, *et al.*, "A dosimetric comparison of lattice, brass, and proton grid therapy treatment plans," Pract. Radiat. Oncol. **12**, e442–e452 (2022).
12. X. Fan, Z. Jiang, T. Dai, and Y. Yin, "Dosimetric implications of pvdr definition in photon and proton lattice radiotherapy for large tumors," Int. J. Radiat. Oncol. Biol. Phys. **126**, e452 (2026).
13. A. Prado, J. Martí, P. G. de Acilu, *et al.*, "Dosimetrical and geometrical parameters in single-fraction lattice radiotherapy for the treatment of bulky tumors: Insights from initial clinical experience," Phys. Medica **123**, 103408 (2024).
14. G. A. Croes, "A method for solving traveling-salesman problems," Oper. research **6**, 791–812 (1958).
15. D. J. Rosenkrantz, R. E. Stearns, and P. M. Lewis, II, "An analysis of several heuristics for the traveling salesman problem," SIAM journal on computing **6**, 563–581 (1977).
16. S. Duriseti, J. A. Kavanaugh, J. Szymanski, *et al.*, "Lite sabr m1: A phase i trial of lattice stereotactic body radiotherapy for large tumors," Radiother. Oncol. **167**, 317–322 (2022).
17. Q. Liu, S. Wei, H. Peng, *et al.*, "A multi-source feature-driven deep learning method to generate linear energy transfer distribution for proton therapy," Med. Phys. **52**, e70068 (2025).
18. C. Shang, G. Evans, M. Rahman, and L. Lin, "Beam characteristics of the first clinical 360° rotational single gantry room scanning pencil beam proton treatment system and comparisons against a multi-room system," J. Appl. Clin. Med. Phys. **21**, 266–271 (2020).
19. P. Li, X.-L. Fei, P.-B. He, *et al.*, "Dosimetric verification on himm at the wuwei heavy ion therapy center using anthropomorphic phantoms," Radiat. Phys. Chem. **218**, 111644 (2024).
20. Y. Xia, Y. Lai, K. Wang, *et al.*, "Initial validation and commissioning experience of phoenix plan treatment planning system for scanned carbon ion beams delivered by heavy ion medical machine," Zeitschrift für Medizinische Physik (2026).

21. G. Ferini, P. Castorina, V. Valenti, *et al.*, "A novel radiotherapeutic approach to treat bulky metastases even from cutaneous squamous cell carcinoma: its rationale and a look at the reliability of the linear-quadratic model to explain its radiobiological effects," Front. oncology **12**, 809279 (2022).
22. Y.-N. Zhu, W. Zhang, J. Setianegara, *et al.*, "Proton arc based lattice radiation therapy: feasibility study, energy layer optimization and let optimization," Phys. Med. & Biol. **69**, 215027 (2024).
23. Z. Zuo, Z. Liu, Q. Zhang, *et al.*, "Systematic parameter selection of carbon ion lattice radiation therapy: balancing rbe-weighted dose and letd distributions," Phys. Med. Biol. (2026).
24. M. Janson, L. Glimelius, A. Fredriksson, *et al.*, "Treatment planning of scanned proton beams in raystation," Med. Dosim. **49**, 2–12 (2024).
25. J. Sangster, M. Taylor, D. Jolly, *et al.*, "A rule-based, feedback-driven framework for fully automated prostate vmat planning," J. Appl. Clin. Med. Phys. **27**, e70751 (2026).

Supplementary Files

This is a list of supplementary files associated with this preprint. Click to download.

- 3.SupplementaryMaterials.pdf